This article has been accepted for publication in a future issue of this journal, but has not been fully edited. Content may change prior to final publication. Citation information: DOI 10.1109/LPT.2014.2375337, IEEE Photonics Technology Letters

Simultaneous Refractive Index and Temperature Measurement with LPFG and Liquid-Filled PCF

Guolu Yin, Yiping Wang, *Senior Member*, *IEEE*, Changrui Liao, Bing Sun, Yingjie Liu, Shen Liu, Qiao Wang, Kaiming Yang, Jian Tang, and Xiaoyong Zhong

***Abstract*—We proposed and demonstrated a novel scheme for simultaneous measurement of temperature and refractive index (RI) by cascading a liquid-filled photonics crystal fiber (PCF) to a long period fiber grating (LPFG) written in a single mode fiber. The liquid-filled PCF showed a high temperature sensitivity of 1.695 nm/°C, which is two orders of magnitude higher than that of the LPFG (0.0642 nm/°C). The LPFG exhibited a "blue shift" with the increased RI. In contrast, liquid-filled PCF showed a total immunity to the surrounding RI. So the temperature was solely measured by the liquid-filled PCF, and the RI information was extracted from the total response of the LPFG with the temperature effect having been compensated by the liquid-filled PCF.**

***Index Terms*—Optical fiber sensors, Long period fiber grating, Photonic crystal fiber**

I. Introduction

REFRACTIVE index (RI) is an important physical parameter in many applications [1-5], such as water quality monitoring, solution concentration measuring, food quality controlling, etc. Since the RI of solution has a strong dependence on temperature, it is essential to measure simultaneously temperature and RI in practical applications. In order to meet such requirements, a few techniques based on long period fiber gratings (LPFGs) have been proposed by using a surface LPFG inscribed on a D-shaped photonic crystal fiber (PCF) [6], a two-section LPFG with an Ag-coated LPFG section and a bare LPFG section [7], a LPFG with ultra-long period of several millimeters [8], and a LPFG inscribed on a concatenated double-clad and single-clad fiber [9]. However, the complicated fabrication process of these specialty LPFGs restricts their practical applications. Alternative schemes are to cascade another sensing element, e.g. fiber Bragg grating [10], Fabry-Perot interferometer [11, 12], S-taper Mach-Zehnder interferometer [13], PCF-based modal interferometer [14], multimode fiber-based modal interferometer [15], or a small core fiber-based modal interferometer [16], to a LPFG for temperature compensation. The difference of temperature sensitivity between the LPFG and these cascaded elements usually is relative small and almost on the same order of magnitude, which limits the accuracy of temperature compensation. Furthermore, the modal interferometers suffer from a low accuracy of the peak wavelength determination because the peak profiles result from the interference between the fundamental mode and uncertain cladding modes [17, 18].

In this paper, we proposed and demonstrated a novel temperature compensation scheme by cascading a liquid-filled PCF to a LPFG. The bandgap edge of the liquid-filled PCF was strongly influenced by temperature due to thermal-optic effect of the filled liquid, whereas it is almost independent of the surrounding RIs because the light is well bounded in the core region. Thus, the liquid-filled PCF was developed to compensate for the temperature effect in case a LPFG was used for RI sensing. Compared with the reported LPFG-based cascaded device [10-16], the proposed scheme has two main advantages. Firstly, the resonant dip of the LPFG and the bandgap edge of the liquid-filled PCF has a wavelength separation of 130 nm, which is large enough to avoid the optical crosstalk. Secondly, the temperature sensitivity of the liquid-filled PCF was two orders of magnitude higher than that of the LPFG. To the best of our knowledge, it is the maximum difference of the temperature sensitivities between two sensing elements in the LPFG-based structures. Such temperature difference improves the accuracy of temperature compensation.

II. Device Fabrication

Our proposed sensor structure consists of a LPFG and a liquid-filled PCF, as shown in Fig. 1(a). The LPFG was inscribed in a standard single mode fiber (SMF) (Yangtze Optical Fiber and Cable Co., Ltd.) by use of a commercial splicer machine (Fujikura, ARC master FSM-100P+) with our improved arc discharge technique [19, 20]. Firstly, the standard SMF with a short unjacketed section was positioning between the electrodes by means of the two fiber holders of the splicer. Secondly, arc discharge with a current of 13 mA and duration of 6 s was performed to induce refractive index modulation in the fiber. Thirdly, the fiber was moved by a grating pitch of 610 μm via the SWEEP motor of the splicer. Afterwards, the second

This work is supported by the National Science Foundation of China (grants no. 61405128, 11174064, 61308027, and 61377090), the Science & Technology Innovation Commission of Shenzhen (grants no. KQCX 20120815161444632 and JCYJ 20130329140017262), China Postdoctoral Science Foundation funded project (grant no. 2014M552227), and the Distinguished Professors Funding from Shenzhen University and Guangdong Province Pearl River Scholars.

All authors are with Key Laboratory of Optoelectronic Devices and Systems of Ministry of Education and Guangdong Province, College of Optoelectronic Engineering, Shenzhen University, Shenzhen 518060 , China (e-mail: glyin@szu.edu.cn and ypwang@szu.edu.cn).

This article has been accepted for publication in a future issue of this journal, but has not been fully edited. Content may change prior to final publication. Citation information: DOI 10.1109/LPT.2014.2375337, IEEE Photonics Technology Letters

and third steps were repeated 28 times. Consequently, a LPFG without visible physical deformation was achieved.

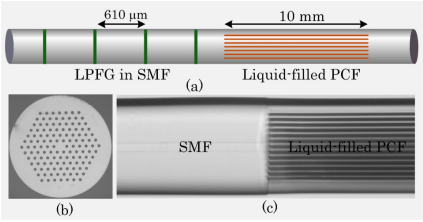

Fig. 1 (a) Schematic diagram of the cascaded fiber device consisting of a LPFG and a liquid-filled PCF, (b) cross-section image of the PCF, (c) spliced section of the PCF with a SMF.

A broadband amplified spontaneous emission (ASE) light source with a wavelength range from 1250 to 1650 nm and an optical spectrum analyzer (YOKOGAWA, AQ6370C) with a wavelength resolution of 0.02 nm were employed to measure the transmission spectra of our proposed devices. As shown in Fig. 2(a), four resonant dips are observed in the transmission spectrum of the LPFG. The resonant dip at 1481 nm has a maximum attenuation up to 30 dB. In order to determine the corresponding cladding mode of the resonant dip, another LPFG was inscribed with the same grating parameter. The inset in Fig. 2(a) illustrates the near mode field pattern at 1481 nm measured by use of a near-infrared camera. The intensity distribution indicates that the resonant dip at 1481 nm corresponds to the coupling from the fundamental mode to the LP_{14} cladding mode.

Furthermore, large-mode-area pure silica PCF (ESM-12, NKT) with a core diameter of about 12 μm was employed to fabricate a liquid-filled PCF sample. Air holes with a diameter of 3.3 μm are arranged in a hexagonal pattern with a pitch of 7.4 μm, as shown in Fig. 1(b). Firstly, a section of PCF with a length of 10 mm was prepared by cleaving two ends of the PCF. Secondly, one end of the PCF was immersed into liquid oil (refractive index matching liquid from Cargille Labs) with a RI of 1.698 at 589.3 nm at 25 °C and a thermo-optic coefficient of -4.79×10^{-4}/°C. After 5 minutes, the air holes of the 10 mm PCF were fully filled with well-known capillary action. Finally, two ends of the liquid-filled PCF were spliced with SMFs by using a commercial arc fusion splicer (Fujikura FSM-60S), as described below.

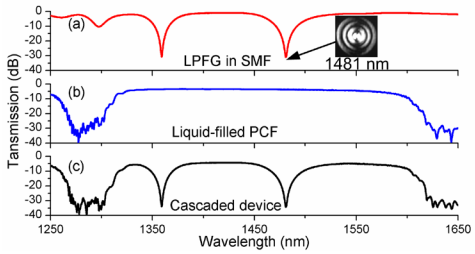

Fig. 2 Transmission spectra of (a) the LPFG, inset: the near mode field pattern of LP_{14} cladding mode at 1481 nm (b) the liquid-filed PCF, and (c) the cascaded LPFG and liquid-filled PCF device

The major challenge of splicing the SMF and the liquid-filled PCF is maybe resulting in bubble in the splicing joint due to the gasification of the liquid material. In order to solve this problem, we preliminarily removed the liquid material at the end of the liquid-filled PCF before splicing. The way of removing the liquid is to perform the cleaning arc discharge with a short duration of 50 ms for several times at the end of the liquid-filled PCF. On the one hand, the arc discharge can gasify the liquid, and on the other, the short duration is not enough to collapse the air hole of the PCF. After the pre-processing above, we spliced the liquid-filled PCF to a SMF by making a 30 μm offset from the joint to the central axis of arc discharge in order to apply a smaller heat amount to the PCF than the SMF [21]. After several trials, the total insertion loss of two splicing joints is around 4 dB. Fig. 1(c) shows the microscope image of the spliced section, where the smooth splicing joint and non evident collapse of the holes indicate that the light in SMF is well coupled into the liquid-filled PCF.

Fig. 2(b) illustrates the transmission spectrum of the liquid-filled PCF. As shown in Fig. 2(b), one bandgap with an extinction ratio of 30 dB occurred in the wavelength range the transmission spectrum from 1250 to 1650 nm. Here, the liquid-filled PCF can be considered as a fiber where the pure silica core is surrounded by a finite array of high-index rods. Because the RI of the liquid rods (1.698 at 589.3 nm) is much larger than that of the silica (1.444 at 1550 nm), the effective RI of the cladding is higher than that of the core. As a result, the index-guided PCF was transferred into a bandgap-guided photonics bandgap fiber (PBF). Thus, the light guidance mechanism in the liquid-filled PCF can be described as photonic bandgap effects [22] [25]. In detail, the light is confined in the pure silica core thanks to the photonic bandgaps which are formed by the periodically arranged liquid rods.

After fabricating the LPFG and the liquid-filled PCF, separately, we constructed the cascaded device by splicing the LPFG and the liquid-filled PCF together. Fig. 2(c) illustrates the transmission spectrum of the cascaded LPFG and liquid-filled PCF device. Two resonant dips of the LPFG were embedded within the bandgap range of the liquid-filled PCF, while the other two resonant dips in the short wavelength direction were attenuated by the band-stop of the liquid-filled PCF. In this work, we selected the resonant dip at 1481 nm and the right bandgap edge for dual parameter sensing.

The most common LPFG-based cascaded device for dual-parameter sensing is usually composed of a LPFG and an interferometer [11-16], which has to face a problem of distinguishing the resonant dip of the LPFG from the fringe pattern of the interferometer because the resonant dip and the fringe pattern are usually inextricably intertwined. Here, our proposed device overcomes this problem by providing a large separation between the resonant dip and the right bandgap edge. In fact, we have much freedom in adjusting the separation by designing the grating pitch of the LPFG and the RI of the filled liquid. According to the phase matching curve of the LPFG [24], the larger the grating pitch is, the longer wavelength the resonant dip locates. On the other hand, the bandgap shifts toward longer wavelength with an increased RI of the filled liquid [23], [25]. Based on the design concept above, we selected the grating pitch of 610 μm and the liquid with RI of 1.698, which results in a 130 nm separation between the resonant dip and the right bandgap edge. Such a separation is

This article has been accepted for publication in a future issue of this journal, but has not been fully edited. Content may change prior to final publication. Citation information: DOI 10.1109/LPT.2014.2375337, IEEE Photonics Technology Letters

large enough to distinguish the resonant dip from the bandgap edge and to avoid the optical crosstalk.

III. Refractive Index and Temperature Responses

To characterize the temperature response of our proposed device, we employed a column oven (LCO 102, ECOM) with a temperature resolution of 0.1 °C to heat the device from room temperature to 90 °C with a step of 10 °C. At each step, the temperature was stabilized at the target values for 10 min, and then the transmission spectrum was recorded. As shown in Fig. 3(a), when temperature was raised, the resonant dip of the LPFG shifted toward a longer wavelength ("red shift"), while the bandgap of the liquid-filled PCF shifted toward a shorter wavelength ("blue shift"). Although the resonant band of LPFG and the bandgap edge of liquid-filled PCF partly overlapped with each other with the rise of temperature, the resonant dip and the banggap edge can still be clearly distinguished.

Fig. 3(b) illustrates the dependence of the wavelength shift on temperature for both the resonant dip of LPFG and the right bandgap edge of liquid-filled PCF. Here, we quantified the wavelength shift of the bandgap edge by tracing the wavelengths, corresponding to -25 dB, of the right bandgap edge at different temperature. Using a linear-regression analysis below

$$\Delta\lambda_{\mathrm{PCF}}^{\mathrm{T}} = 39.202 - 1.695 \times T \tag{1}$$

$$\Delta\lambda_{\mathrm{LFPG}}^{\mathrm{T}} = -1.489 + 0.0642 \times T \tag{2}$$

As shown in Fig. 3(b), the resonant dip of the LPFG has a low temperature sensitivity of 64.2 pm/°C. In contrast, the right bandgap edge of the liquid-filled PCF has a very high temperature sensitivity of 1.695 nm/°C, which is two orders of magnitude higher than that of the LPFG.

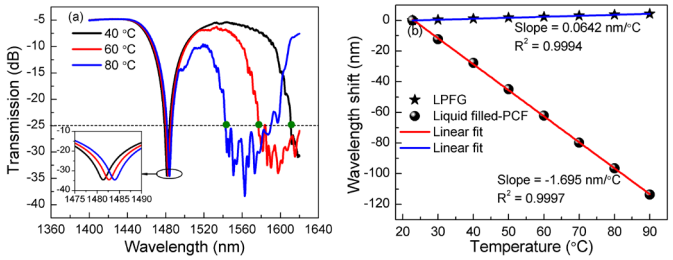

Fig. 3 (a) Transmission spectra of the proposed device at temperatures of 40, 60, and 80 °C, inset: enlarged resonant dip of the LPFG, (b) wavelength shift of the LPFG and the liquid-filled PCF at different temperature.

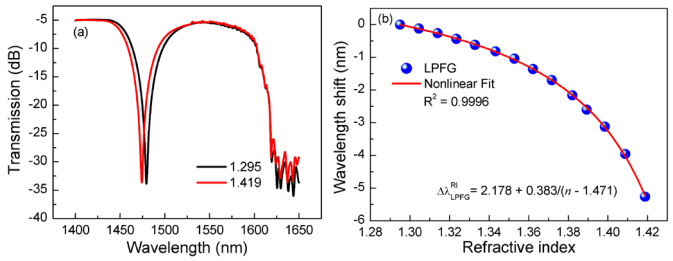

Fig. 4 (a) Transmission spectra of the proposed device immersed in the liquids with a RI of 1.295 and 1.419, (b) resonant wavelength shift of the LPFG at different surrounding RIs.

To characterize the RI performance, we employed a set of refractive index matching liquids (Cargille Labs) with a RI from 1.300 to 1.430 with an interval of 0.01. For each refractive index matching liquid, Cargille Labs gives three RIs at wavelengths of 589.3, 486.1, and 656.3 nm at 25 °C [26]. In order to improve the accuracy of the experimental results, we should calculate the RIs of the liquids at the resonant wavelength of 1481 nm and at the room temperature of 23 °C. Firstly, we applied Cauchy dispersion equation to obtain the RIs at the wavelength of 1481 nm [27]

$$n(\lambda) = C_1 + \frac{C_2}{\lambda^2} + \frac{C_3}{\lambda^4} \tag{3}$$

where the coefficients C_1, C_2 and C_3 can be obtained by substituting the three RIs at wavelengths of 589.3, 486.1, and 656.3 nm to Eq. (3). Secondly, we calculated the RIs at 23 °C by considering the thermal coefficient of each liquid which is also given by Cargille Labs. After that, the labelled refractive indices 1.300 and 1.430 at 589.3 nm at 25 °C are calibrated to be 1.295 and 1.419 at 1481 nm at 23 °C, respectively.

The cascaded LPFG and liquid-filled PCF device was sequentially immersed into different refractive index matching liquids, and then its transmission spectrum was measured. After each measurement, a careful clean-and-dry process was done by using alcohol to remove residual liquid on the device surface until the transmission spectrum comes back to the original one in air. Fig. 4(a) illustrates the transmission spectra of the device at the RIs of 1.295 and 1.419. The resonant wavelength shift of the LPFG was plotted in Fig. 4(b). A nonlinear fitting of the experimental results is as follow.

$$\Delta\lambda_{\mathrm{LPFG}}^{\mathrm{RI}} = 2.178 + 0.383/(n - 1.471) \tag{4}$$

It is found from Fig. 4 that the resonant wavelength of the LPFG exhibits a "blue shift" with the increased RI. In contrast, as shown in Fig. 4(a), the bandgap edge of the liquid-filled PCF was not affected by the surrounding RIs. In other words, the liquid-filled PCF showed a total immunity to the surrounding RI. So the temperature could be solely measured from the spectrum response of the liquid-filled PCF. The surrounding RI could be achieved by means of measuring the resonant wavelength shift of the LPFG with temperature compensation, as described below.

After characterizing the temperature and RI responses of the LPFG and the liquid-filled PCF, separately, we demonstrated the cascaded LPFG and liquid-filled PCF sensor's capability for simultaneous measurement of temperature and surrounding RI. Firstly, the sensor was inserted into a 40 mm-long glass capillary with an inner diameter of 300 μm. Secondly, one end of the capillary tube was immersed into refractive index matching liquid with a RI of 1.35 at 589.3 nm at 25 °C and a thermal coefficient of -3.39 × 10^{-4}/°C, and then the capillary tube was fully filled by the liquid via capillary action. Thirdly, two ends of the capillary tube were sealed with AB glue. The sensor was then placed into the column oven employed in the previous temperature experiments. The transmission spectra of the sensor were recorded at different temperature of 23, 25, 30, 34, 37.9, 42.3, 48.5, 51.7, 58.4, 62.5, and 68.9 °C.

In data processing, first of all, the measured temperature

values were calculated from the bandgap edge shift of the liquid-filled PCF by equation (1). According to the temperature sensitivity of the liquid-filled PCF illustrated in Fig. 3(b) and the OSA resolution of 0.02 nm, the theoretic temperature resolution of the proposed sensor is 0.01 °C. Therefore the measured temperature values agreed well with the setting values with a resolution of 0.1 °C. Due to ripples on the bandgap edge which was caused most probably by interference of the fundamental mode and the surface modes, a realistic temperature measurement resolution was estimate around 0.1 °C in the practical application.

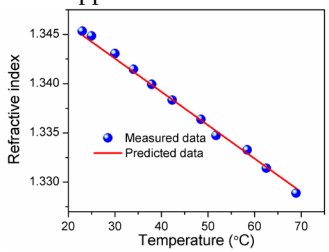

Fig. 5 Variation of the RI of a refractive index matching liquid with temperature.

After obtaining the measured temperature values, the temperature-induced wavelength shift of the LPFG was calculated by equation (2) and then subtracted from the total resonant wavelength shift of the LPFG, leaving a net wavelength shift resulting from the surrounding RI. Finally, the surrounding RIs were calculated from equation (4) and plotted in Fig. 5 by sphere symbols. Furthermore, the predicated RIs around the wavelength of 1480 nm at different temperatures were calculated by the Cauchy equation and the thermal coefficient of the liquid, and then depicted in Fig. 5 by a solid line. Compared with the measured and predicted RIs, the average error is ~3.03×10^{-4}, and the standard deviation is ~2.01×10^{-4}.

IV. Conclusion

In conclusion, a novel scheme was proposed and demonstrated for simultaneous measurement of temperature and RI by means of cascading a liquid-filled PCF to a LPFG. The dual-parameter sensing ability of the device originates from the sole temperature response of the liquid-filled PCF, which is used to compensate for the temperature contribution in the total spectral response of the LPFG, leaving a net effect resulting from the surrounding RI. The simultaneous measurement of temperature and surrounding RI was experimentally demonstrated and showed a good agreement with actual values.

References

1. S. Singh, "Refractive index measurement and its applications," *Physica Scripta*, vol. 65, no. 2, pp. 167-180, 2002.
2. L. Mosquera, D. Sáez-Rodriguez, J. L. Cruz, and M. V. Andrés, "In-fiber Fabry-Perot refractometer assisted by a long-period grating," *Opt. Lett.*, vol. 35, no. 4, pp. 613-615, 2010.
3. Y. P. Wang, "Review of long period fiber gratings written by CO_2 laser," *Journal of Applied Physics*, vol. 108, no. 8, pp. 081101-1-081101-18, 2010.
4. A. Pliss, L. L. Zhao, T. Y. Ohulchanskyy, J. L. Qu, and P. N. Prasad, "Fluorescence Lifetime of Fluorescent Proteins as an Intracellular Environment Probe Sensing the Cell Cycle Progression," *Acs Chemical Biology*, vol. 7, no. 8, pp. 1385-.1392, 2012.
5. Z. Li, Y. Wang, C. Liao, S. Liu, J. Zhou, X. Zhong, Y. Liu, K. Yang, Q. Wang, and G. Yin, "Temperature-insensitive refractive index sensor based on in-fiber Michelson interferometer," *Sensors and Actuators B-Chemical*, vol. 199, pp. 31-35, Aug 2014.
6. H. J. Kim, O. J. Kwon, S. B. Lee, and Y. G. Han, "Polarization-dependent refractometer for discrimination of temperature and ambient refractive index," *Opt. Lett.*, vol. 37, no. 11, pp. 1802-1804, 2012/06/01 2012.
7. T. Allsop, R. Neal, D. Giannone, D. J. Webb, D. J. Mapps, and I. Bennion, "Sensing Characteristics of a Novel Two-Section Long-Period Grating," *Appl. Opt.*, vol. 42, no. 19, pp. 3766-3771, 2003/07/01 2003.
8. T. Zhu, Y.-J. Rao, and Q.-J. Mo, "Simultaneous measurement of refractive index and temperature using a single ultralong-period fiber grating," *IEEE Photon. Technol. Lett.*, vol. 17, no. 12, pp. 2700-2702, 2005.
9. Q. Han, X. W. Lan, J. Huang, A. Kaur, T. Wei, Z. Gao, and H. Xiao, "Long-period grating inscribed on concatenated double-clad and single-clad fiber for simultaneous measurement of temperature and refractive index," *IEEE Photon. Technol. Lett.*, vol. 24, no. 13, pp. 1130-1132, 2012.
10. X. Shu, B. A. L. Gwandu, Y. Liu, L. Zhang, and I. Bennion, "Sampled fiber Bragg grating for simultaneous refractive-index and temperature measurement," *Opt. Lett.*, vol. 26, no. 11, pp. 774-776, 2001/06/01 2001.
11. D. W. Kim, F. Shen, X. Chen, and A. Wang, "Simultaneous measurement of refractive index and temperature based on a reflection-mode long-period grating and an intrinsic Fabry-Perot interferometer sensor," *Opt. Lett.*, vol. 30, no. 22, pp. 3000-3002, 2005/11/15 2005.
12. C.-L. Lee, W.-F. Liu, Z.-Y. Weng, and F.-C. Hu, "Hybrid AG-FFPI/RLPFG for Simultaneously Sensing Refractive Index and Temperature," *IEEE Photon. Technol. Lett.*, vol. 23, no. 17, pp. 1231-1233, 2011.
13. J. L. Li, W. G. Zhang, S. C. Gao, P. C. Geng, X. L. Xue, Z. Y. Bai, and H. Liang, "Long-Period Fiber Grating Cascaded to an S Fiber Taper for Simultaneous Measurement of Temperature and Refractive Index," *IEEE Photon. Technol. Lett.*, vol. 25, no. 9, pp. 888-891, 2013.
14. D. J. Juan Hu, J. L. Lim, M. Jiang, Y. Wang, F. Luan, P. Ping Shum, H. Wei, and W. Tong, "Long period grating cascaded to photonic crystal fiber modal interferometer for simultaneous measurement of temperature and refractive index," *Opt. Lett.*, vol. 37, no. 12, pp. 2283-2285, 2012/06/15 2012.
15. J. Huang, X. Lan, A. Kaur, H. Wang, L. Yuan, and H. Xiao, "Temperature compensated refractometer based on a cascaded SMS/LPFG fiber structure," *Sensors and Actuators B: Chemical*, vol. 198, no. 0, pp. 384-387, 2014.
16. Q. Wu, H. P. Chan, J. Yuan, Y. Ma, M. Yang, Y. Semenova, Y. Binbin, P. Wang, C. Yu, and G. Farrell, "Enhanced refractive index sensor using a combination of a long period fiber grating and a small core singlemode fiber structure," *Measurement Science and Technology*, vol. 24, no. 9, p. 094002, 2013.
17. Y. Li, E. Harris, L. Chen, and X. Y. Bao, "Application of spectrum differential integration method in an in-line fiber Mach-Zehnder refractive index sensor," *Opt. Express*, vol. 18, no. 8, pp. 8135-8143, 2010.
18. G. Yin, S. Lou, and H. Zou, "Refractive index sensor with asymmetrical fiber Mach–Zehnder interferometer based on concatenating single-mode abrupt taper and core-offset section," *Optics & Laser Technology*, vol. 45, pp. 294-300, 2013.
19. G. Yin, Y. Wang, C. Liao, J. Zhou, X. Zhong, G. Wang, B. Sun, and J. He, "Long Period Fiber Gratings Inscribed by Periodically Tapering a Fiber," *IEEE Photon. Technol. Lett.*, vol. 26, no. 7, pp. 698-701, Apr 1 2014.
20. G. Yin, Y. Wang, C. Liao, J. Zhou, X. Zhong, S. Liu, Q. Wang, Z. Li, B. Sun, J. He, and G. Wang, "Improved arc discharge technique for inscribing compact long period fiber gratings," in *23rd International Conference on Optical Fiber Sensors*, Proc. SPIE, 2014, vol. **9157**, pp. 91577X-1
21. L. Xiao, M. S. Demokan, W. Jin, Y. Wang, and C. Zhao, "Fusion Splicing Photonic Crystal Fibers and Conventional Single-Mode Fibers: Microhole Collapse Effect," *J. Lightwave Technol.*, vol. 25, no. 11, pp. 3563-3574, 2007/11/01 2007
22. Y. Wang, X. Tan, W. Jin, D. Ying, Y. Hoo, and S. Liu, "Temperature-controlled transformation in fiber types of fluid-filled photonic crystal fibers and applications," *Opt. Lett.*, vol. 35, no. 1, pp. 88-90, 2010/01/01 2010.
23. Y. Liu, Y. Wang, B. Sun, C. Liao, J. Song, K. Yang, G. Wang, Q. Wang, G. Yin, and J. Zhou, "Compact tunable multibandpass filters based on liquid-filled photonic crystal fibers," *Opt. Lett.*, vol. 39, no. 7, pp. 2148-2151, 2014/04/01 2014.
24. A. M. Vengsarkar, P. J. Lemaire, J. B. Judkins, V. Bhatia, T. Erdogan, and J. E. Sipe, "Long-period fiber gratings as band-rejection filters," *J. Lightwave Technol.*, vol. 14, no. 1, pp. 58-65, 1996.
25. B. T. Kuhlmey, B. J. Eggleton, and D. K. C. Wu, "Fluid-Filled Solid-Core Photonic Bandgap Fibers," *J. Lightwave Technol.*, vol. 27, no. 11, pp. 1617-1630, 2009.
26. "Introduction to Optical Liquids" (Cargille Labs), http://www.cargille.com/opticalintro.shtml.
27. S. C. Su, F. D. Bloss, and M. Gunter, "Procedures and computer programs to refine the double variation method," *American Mineralogist*, vol. 72, pp. 1011-1013, 1987.